

MEASUREMENTS OF DRAG TORQUE, LIFT OFF SPEED, AND STRUCTURAL PARAMETERS IN A 1ST GENERATION FLOATING GAS FOIL BEARING

Luis San Andrés
Mast-Childs Professor
Texas A&M University
Mechanical Engineering Dept.
College Station, Texas 77843

José Camero
Undergraduate Student
University of Texas at San Antonio
Mechanical Engineering Dept.
San Antonio, Texas 78249

Shane Muller
Undergraduate Student
Calvin College
Mechanical Engineering Dept.
Grand Rapids, MI 49546

Thomas Chirathadam
Research Assistant
Texas A&M University
Mechanical Engineering Department
College Station, Texas 77843-3123

Keun Ryu
Research Assistant

ABSTRACT

Gas foil bearings (GFBs) in oil-free microturbomachinery enable low maintenance and near frictionless performance, thus reducing operating cost and increasing overall system efficiency. Empirical characterization of foil bearing performance is still relevant in lieu of the limitations of analytical GFB models to predict reliable data, in particular for lift-off speed, power loss and ultimate load capacity. Presently, varying rotor speed tests with increasing external loads applied on a 1st generation GFB serve to identify the bearing lift off speed and drag torque during recurrent start and shut down events. The test rig comprises of a commercial turbocharger air turbine driving a test journal (36.512 mm in OD) and floating gas foil bearing (weight = 10.27 N, length=38.1 mm) mounted on the compressor side. A thermoplastic resin-bonded PTFE coating (16 μm thick) on the journal ensures low friction, albeit its durability is not suited for extended operation. Upon completion of the test series, visual inspection reveals the rotor OD is denuded of its coating with the top foil showing polished wear marks. The GFB drag torque during dry friction sliding operation (start-up and shut down) increases with the applied load, max 53 N. The bearing drag torque during rotor shut down is ~20% lesser than the break away torque during start up. Once airborne, typically at 12 krpm and above, the GFB drag torque is small and remains fairly constant -regardless of the applied load- to the largest operating speed of 45 krpm. Prior to bearing lift off, the drag power loss increases rapidly with rotor speed. Once airborne, the bearing power loss remains relatively constant even as the journal speed increases. Large static loads also cause larger power losses (75 W on average). Other tests conducted with an electro magnetic shaker aim to determine the foil bearing structural stiffness and damping coefficients, both frequency and amplitude dependent. The structural loss factor, best to describe the mechanical energy dissipation characteristics of a foil bearing, decreases with frequency, and its magnitude at just 0.3 and lesser is typical for a first generation foil bearing.

INTRODUCTION

Gas foil bearings (GFBs) are compliant surface hydrodynamic bearings using ambient air as the working fluid

media. GFBs enable microturbomachinery to operate at high speed and high temperature with significant reduction in power loss and increase in system thermal efficiency. Oil-free systems have lesser part count, footprint and weight and are environmentally friendly with demonstrated savings in long-interval maintenance expenses. Lightly loaded turbocompressors and microturbines implement GFBs as low-friction rotor support elements [1,2].

Successful implementation of GFBs in commercial rotating machinery involves a two-tier effort; that of developing bearing structural components and solid lubricant coatings to improve the bearing load carrying capacity with reduced friction, and that of developing accurate performance prediction models anchored to reliable (non commercial) test data. Chen et al. [3] and DellaCorte et al. [1] publicize details on the design and construction of first generation foil bearings aiming towards their wide adoption in industry.

Since 2003, research at TAMU Turbomachinery Laboratory focuses on advancing computational tools, experimentally validated, to predict the static and dynamic forced performance of GFBs. References [4-10], representative of the research progress to date, include methods and test rigs for the identification of FB structural stiffness and damping coefficients from static and dynamic load tests [4-8], test rigs and measurements to quantify the effects of FB structure nonlinearity [9,10], side pressurization [11], mechanical preload [12] and shaft temperature [13] on the dynamic forced response and stability of a rotor supported on 2nd generation GFBs. The program targeting high temperature applications, such as in gas turbines, has also developed a GUI based thermoelastohydrodynamic computational model [14], currently licensed to various OEMs. Extensive laboratory test data aided to benchmark the predictive tool, see Refs. [4-14].

Importantly enough, the education of engineering students in this emerging field is of utmost importance when considering the preeminent role envisioned for distributed power generation with alternative and sustainable sources such as fuel cells, for example. Hence, since 2007, the research program at TAMU, with funding from NSF (REUP), has educated mechanical engineering undergraduate students in advanced gas bearing technology. The ten week summer

program, with students selected from a nation wide pool targeting minorities (gender and race), has been successful. Reference [15] reports the work completed by four students in the Summer of 2008 with details on the design and manufacturing of bump strip layers for FBs, the measurement and prediction of rotordynamic response in a rotor supported on GFBs, and the evaluation of the start-up and shut-down performance of a rotor supported on metal mesh FBs.

This paper details the research conducted by two undergraduate students in Summer 2009. Seasoned graduate students working in the laboratory guided the students during the fast pace program. The students' research focused on the characterization of first generation FBs donated by KIST (Korea Institute of Science and Technology). The work aims to deliver reliable experimental data for the tested FBs to further benchmark the physics-based computational model, while also providing the students an opportunity to learn about safety and shop practices, the operation of measurement sensors and data acquisition systems, and analysis of experimental results including estimation of uncertainties, etc.

NOMENCLATURE

C_{eq}	FB equivalent viscous damping [N-s/m]
D	$=2R$. Journal outer diameter [m]
D_i, D_o	FB shell inner and outer diameters [m]
D_T	Top foil inner diameter [m]
$F(\omega)$	External dynamic force applied to FB [N]
f	$= T_{or}/WR$. FB friction or drag coefficient [-]
h_B, r_B	Bump foil height and curvature radius [m]
$H(\omega)$	FB mechanical impedance [N/m]
K	FB structural stiffness [N/m]
L	FB axial length [0.0381 m]
l_B	Bump foil length [m]
M	FB test bearing mass [kg]
s_o	Bump foil pitch [m]
T_{or}	FB drag torque [N-m]
t_B, t_T	Bump foil and top foil thickness [m]
W	Static load applied on bearing [N]
$X(\omega)$	FB dynamic displacement [m]
α	Bump foil arc angle [deg]
γ	$=C_{eq}\omega/K$. FB structural loss factor [-]
ϕ	$=T_{or}\Omega$. FB power loss [W]
Ω	Rotor speed [rad/s]
ω	Excitation frequency [rad/s]
ω_n	Test bearing system natural Frequency [rad/s]

ACRONYMS

DOF	Degree of freedom
GFB	Gas foil bearing
ID, OD	Inner diameter, Outer diameter
PTFE	Poly Tetra Fluor Ethylene
TC	Turbocharger

DESCRIPTION OF TEST FOIL BEARING

Figure 1 depicts a photograph of the first-generation test foil bearing¹ and Table 1 details its geometry and material characteristics. The bearing comprises of a single arcuate top

¹ The test bearing is one of a set of bearings and rotor donated by KIST for educational research. See Ref. [16] for details on the items donated.

foil and a single bump arcuate foil bump strip layer wrapped around the ID of a bearing shell. The bare (uncoated) foils are made of Inconel X-750. The ends of both foils slide into an angled slot in the bearing cartridge and fastened with hex screws. This design feature allows for rapid assembly or disassembly and replacement of parts, if needed.

Table 1. Geometry of 1st gen. test foil bearing [16]

Parameter	Magnitude
Number of bumps	26
Bearing shell outer diameter, D_o	50.8 mm
Bearing shell inner diameter, D_i	37.95 mm
Bearing axial length, L	38.10 mm
Top foil thickness, t_T	0.12 mm
Bump foil thickness, t_B	0.12 mm
Top foil inner diameter, $D_T = D_i - 2(t_T + h_B)$	36.630 mm
Bump pitch, s_o	4.3 mm
Bump length, l_B	2.1 mm
Bump height, h_B	0.54 mm
Bump arc radius, r_B	2.5 mm*
Bump arc angle, α	50 deg*
Journal OD: tests for FB structural parameters	36.555 (uncoated)
Journal OD: tests with rotation, TC test rig	36.512 (uncoated) 36.544 (coated)

* Estimated from zoomed photograph, see Fig. 1

1) Materials: Inconel X-750 for bump strip layer and top foil, AISI 4140 for bearing shell

2) Bearing weight 0.27 kg (shell and foils)

IDENTIFICATION OF STRUCTURAL STIFFNESS AND DAMPING IN A 1ST GENERATION FOIL BEARING

The ultimate load capacity of a GFB depends on the structural properties and geometry of the underlying bump strip layers. Hence, the need for an accurate knowledge of the mechanical properties, namely stiffness and damping, of the FB underspring support. Figure 2 depicts a photograph of the set up for measurement of foil bearing deflection due to dynamic loads applied with an external shaker. The foil bearing is press fitted into a thick bearing cartridge² that incorporates sensors for measurement of bearing acceleration and the applied load. The bearing assembly, weighing 0.945 kg, slides into a rigid³ and stationary AISI 4140 solid shaft, 36.555 mm in outer diameter. The bearing is installed with the top foil end at 45° from the horizontal plane, as shown in the schematic view in Fig. 2.

A small electromagnetic shaker, flexibly mounted, applies single frequency loads on the bearing assembly, and an eddy current sensor facing the bearing housing OD records the ensuing dynamic displacement. In the tests, conducted at ambient temperature of 21 °C, the excitation frequency (ω) varied from 50 Hz to 200 Hz, with a frequency step of 10 Hz. A Virtual Instrument and controller available in the laboratory

² Most commercial bearing cartridges have thin walls; better referred as a bearing shell. Enlarging the diameter of the bearing ensures that the imposed external loads do not deform the bearing ring but only the bumps when pushed against the stationary shaft.

³ The shaft is rigidly affixed to thick pedestals. Shaft deflections at the location of the bearing are negligible with respect to those of the elastic structure in the foil bearing. The near rigid shaft condition is paramount to obtain reliable data with a minimum of instrumentation, see Refs. [4-8].

adjusts automatically the amplitude of the applied shaker load to obtain pre-set bearing displacements with amplitudes at 38, 57 and 76 μm . Note that FB structural force coefficients are amplitude and frequency dependent [5-8], hence the need to keep one of the variables fixed while the other varies.

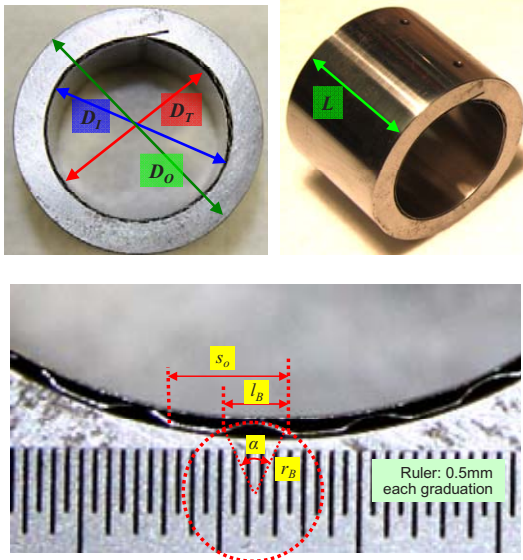


Fig. 1 Photographs of first-generation foil bearing. Noted dimensions measured or estimated [16]

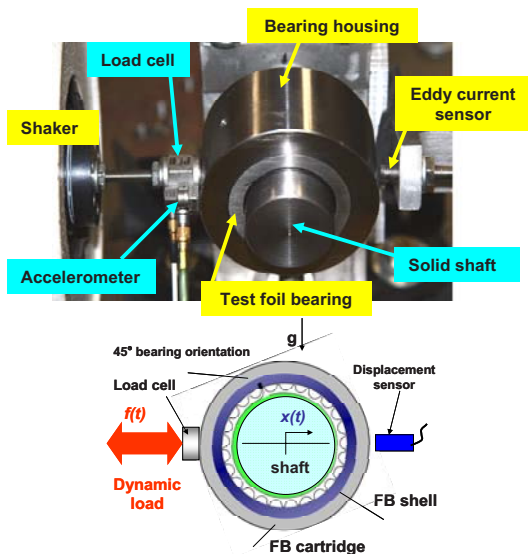


Fig. 2 Photograph and schematic view of test setup for dynamic load and foil bearing deflection measurements. Stationary (non rotating) rigid shaft

Figure 3 depicts typical waterfalls of applied load and ensuing FB displacement with amplitude equal to 57 μm . In general, the dynamic load increases with frequency. However, the load magnitude drops markedly for excitations with a frequency coinciding with the bearing system natural frequency at ~ 90 Hz. The smallness of the applied load at this frequency denotes the FB has little damping. Incidentally,

note that the recorded FB displacements show negligible excitation of displacements at higher order frequencies (multiples of excitation frequency), thus denoting the test FB system is linear.

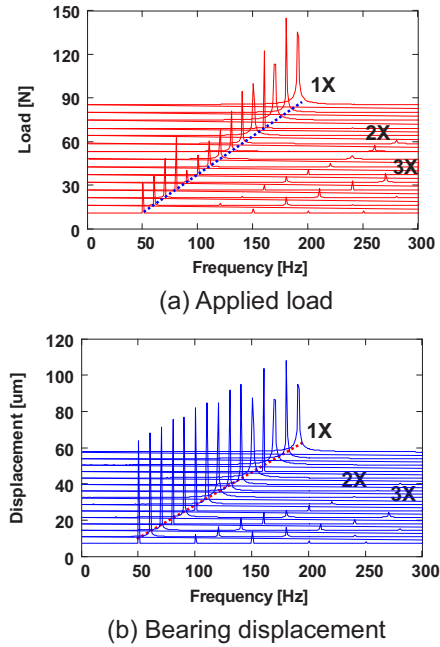


Fig. 3 Waterfall of (a) applied load and (b) foil bearing displacement versus excitation frequency. Set FB motion amplitude at 57 μm

Hence, the test FB system is modeled as a single DOF linear mechanical system with fundamental physical parameters of mass (M), stiffness (K), and equivalent viscous damping (C_{eq}). Processing in the frequency domain of the applied dynamic load $F(\omega)$ and ensuing FB displacement $X(\omega)$ determines the impedance (H) relationship [17]:

$$H(\omega) = \frac{F(\omega)}{X(\omega)} = (K - M\omega^2) + iC_{eq}\omega \quad (1)$$

where ω is the excitation frequency and $i = \sqrt{-1}$. Above, $F(\omega)$ and $X(\omega)$ are complex numbers, whose real and imaginary parts vary with frequency

From the test data in the frequency domain, the FB system parameters follow from curve fits of the real and imaginary parts of the impedance function

$$\begin{aligned} K - M\omega^2 &\leftarrow \text{Real}[H(\omega)]; \\ C_{eq}\omega &\leftarrow \text{Imag}[H(\omega)] \end{aligned} \quad (2)$$

Figure 4 depicts the real part of the mechanical impedance H versus frequency for the three bearing displacements at 38, 57 and 76 μm . Note that the system natural frequency $\omega_n = \sqrt{K/M} \sim 90$ Hz, i.e. the frequency at which $\text{Real}(H)=0$, is invariant to the amplitude of motion. The quadratic curve fit, first of Eq. (2), renders a system mass $M=1.1\sim 1.3$ kg while the physical bearing mass is 0.945 kg.

The ~ 16% difference is not unusual since the test system has added masses from the sensors and connections, for example. Incidentally, the goodness of the fit is $R^2 \geq 0.99$ denoting the physical model is appropriate for the test data.

Note that the measurements were repeated thrice; the maximum variability in results is ~ 49% at frequencies below 90 Hz and ~ 13% in the frequency range from 100 Hz to 200 Hz. Further analysis also determines that the uncertainty in the system impedance is 8% maximum.

Bearing displacements (38 μm to 76 μm) have little influence on the identified system stiffness K , as shown in Fig. 5. However, the bearing structural stiffness shows a peculiar behavior with respect to frequency, with an apparent drop in magnitude just before the system natural frequency, and a subsequent slight raise for higher frequencies. Prior measurements with similar size foil bearings [5-7] did not find the unusual condition. Rationale for the distinct stiffness drop and raise may be due to the small amplitude loads needed to excite the test system around its natural frequency.

Taken aside the region of abrupt changes, the system stiffness K appears quite nearly constant with an average value of ~0.4 MN/m. The noted stiffness magnitude⁴ is within the range of FB structural stiffnesses determined from static load tests as detailed in Ref. [18]. Presently, from three independent tests repeated with identical conditions, the maximum variability in bearing stiffness is ~32% for frequencies below 90 Hz and ~ 22% in the frequency range from 100 Hz to 200 Hz. The uncertainty in the identified bearing stiffness is approximately 10%. Note that a unique system M represents best each test condition.

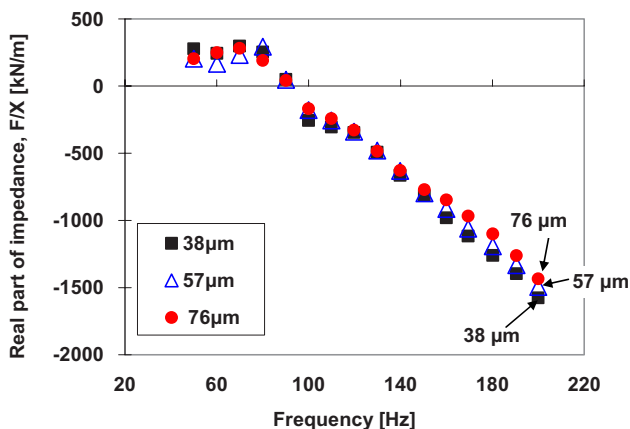


Fig. 4 Real part of FB mechanical impedance H versus excitation frequency. Measurements for three FB displacements at 38, 57 and 76 μm

Figure 6 depicts the identified FB viscous damping C_{eq} decreases rapidly with the excitation frequency. Furthermore, the larger the amplitude of dynamic displacement, the smaller the damping magnitude is. This finding is typical of systems with dry-friction, as in a foil bearing⁵, where in general $C_{eq} \sim 1/(X\omega)$ [19]. From three separate tests repeated under identical conditions, the maximum difference in damping

⁴ A reviewer noted the test FB is fairly soft compared to bearings in commercial use.

⁵ Recall that damping in a foil bearing arises from sliding of the bumps against the bearing ID and against the top foil.

values is ~ 26% for frequencies below <90Hz and 16% in the frequency range from 100Hz to 200Hz. The uncertainty in the estimated damping (C_{eq}) is 8% maximum.

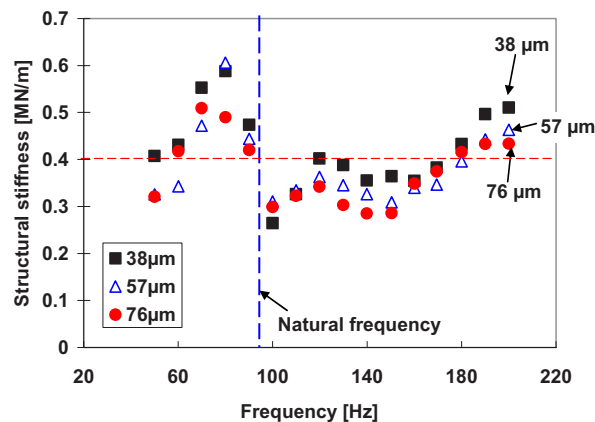


Fig. 5 Identified FB structural stiffness K versus excitation frequency. Measurements for three FB displacements at 38, 57 and 76 μm

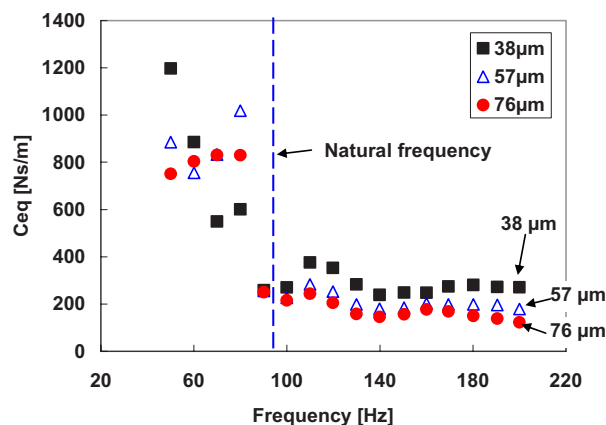


Fig. 6 identified FB viscous damping coefficient C_{eq} versus excitation frequency. Measurements for three FB displacements at 38, 57 and 76 μm

A viscous damping coefficient clearly does not represent the actual mechanical energy dissipation characteristics in a foil bearing. Hence, it is more accurate and physically realistic to model the bearing damping as of material or hysteretic type with a structural loss factor γ , simply related to the viscous damping coefficient by $\gamma = \frac{C_{eq}\omega}{K}$.

Figure 7 shows the identified FB structural loss factor (γ) versus excitation frequency derived from three FB amplitudes of motion. Above the natural frequency, γ drops from 0.3 to 0.1; while below the natural frequency γ is high at ~ 0.80. These findings are unusual though denoting that, for operation at high frequencies, this first generation test FB has lesser structural damping than a similar size 2nd generation FB. For example, in Refs. [5,7], γ ranges from 0.06 to 0.20, and 0.2 to 0.6, respectively. In Ref. [7], γ increases with frequency. On the other hand, in Ref. [5] γ is nearly uniform over the test

frequency range. Do recall that the test bearings in Refs. [5,7] are second generation, i.e., with multiple bump foil strips, axial and circumferential.

Note also that the maximum variability in loss factor from three separate tests is less than 35 for frequencies below 90 Hz and ~ 45% in the frequency range from 100 Hz to 200 Hz. The uncertainty in the estimated loss factor is 19% maximum.

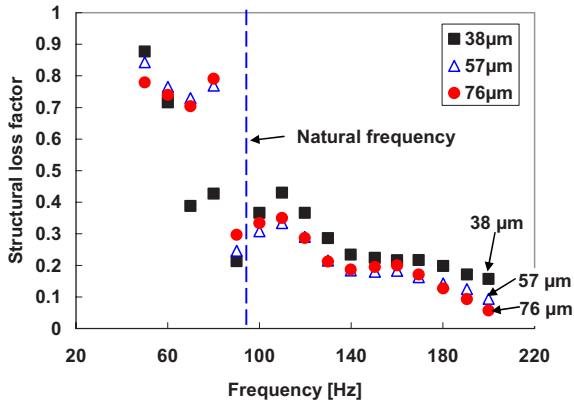


Fig. 7 Identified FB structural loss factor γ versus excitation frequency. Measurements for three FB displacements at 38, 57 and 76 μm

MEASUREMENTS OF LIFT OFF SPEED AND DRAG TORQUE IN A 1ST GEN. GAS FOIL BEARING

Figure 8 portrays a unique test rig for measurement of the start up and shut down response of gas bearings [20]. The rig consists of a commercial turbocharger (TC), supported on oil lubricated ball bearings, whose compressor wheel and casing are removed. An in house fabricated journal fits into the stub of the rotor driven by shop (cold) air supplied to the TC turbine. An AISI 4140 steel journal⁶, 36.514 mm in OD, is coated with a 0.016 mm thick layer of a thermoplastic resin-bonded PTFE coating (PERMALON[®]) following room temperature procedures developed in the laboratory [21]. The test foil bearing assembly, weighing 10.27 N, slides into the coated journal ($D=36.544$ mm) and a torque arm mechanism restrains its rotation, as shown in Fig. 9. The mechanism consists of a long bar with one end inserted into the bearing cartridge and its other end facing a calibrated spring that restrains the bar rotation. An eddy current sensor measures the end displacement of the bar which also denotes the spring elastic deflection, and by proper calibration, gives the drag torque acting on the bearing.

The drag torque is either of dry-friction type when the journal slides in contact with the top foil of the bearing or of hydrodynamic type once bearing lift off is established with a minute gas film separating the bearing from the rotating journal. Figure 9 also shows a simple mechanism to apply pull loads onto the bearing cartridge via a vertical wire that is connected to a hand held dynamometer.

Measurements of the foil bearing drag torque and lift-off journal speed over a range of applied static loads are of importance to determine the bearing power loss and its

reliability to establish near friction-free operation once airborne

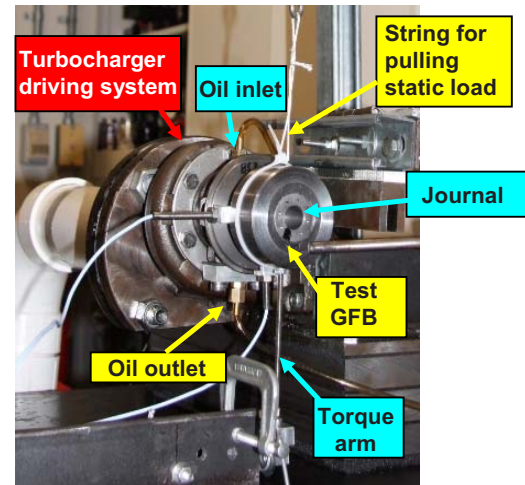


Fig. 8 Turbocharger air turbine driven test rig for measurements of start up response of a floating gas bearing

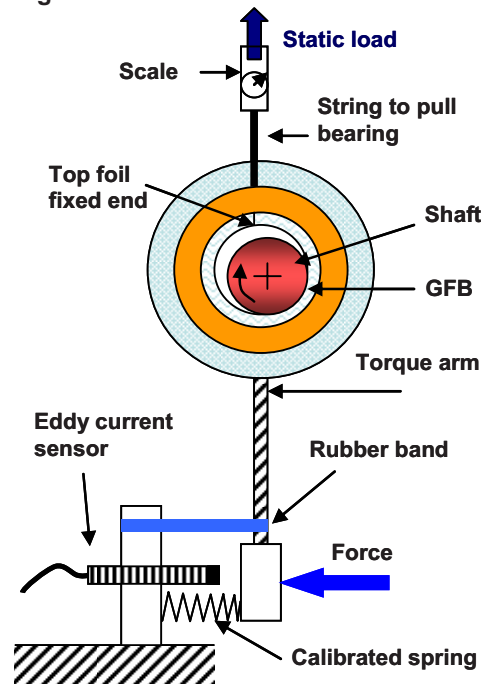


Fig. 9 Schematic view of gas foil bearing in TC turbine driven test rig with torque arm measuring mechanism

Figure 10 depicts typical measurements of drag torque (T_{or}) and rotor speed (Ω) versus elapsed time obtained with the test foil bearing. In the test, a valve supplying air (3 bar gauge pressure) into the TC turbine is slowly opened manually. The external load pulling on the bearing cartridge is also applied at this time. At first, the rotor remains stationary, not overcoming the dry-friction imposed by the foil bearing on its journal. Eventually, as the valve opens more, the turbine

⁶ This journal is different from the one used in the dynamic load tests discussed earlier.

starts turning and the journal slides on the floating bearing. The drag torque quickly reaches a peak. As the rotor speed increases, there is a sudden reduction in torque which denotes bearing lift off and airborne operation with a gas film. For a given valve opening, the rotor will reach a steady state rotational speed. Next, the air supply valve is closed and the rotor immediately begins to coast down. At a certain speed, the rotor deceleration is abrupt thus denoting a touch down condition, with the reappearance of dry-sliding friction which quickly brings the TC turbine to a sudden stop.

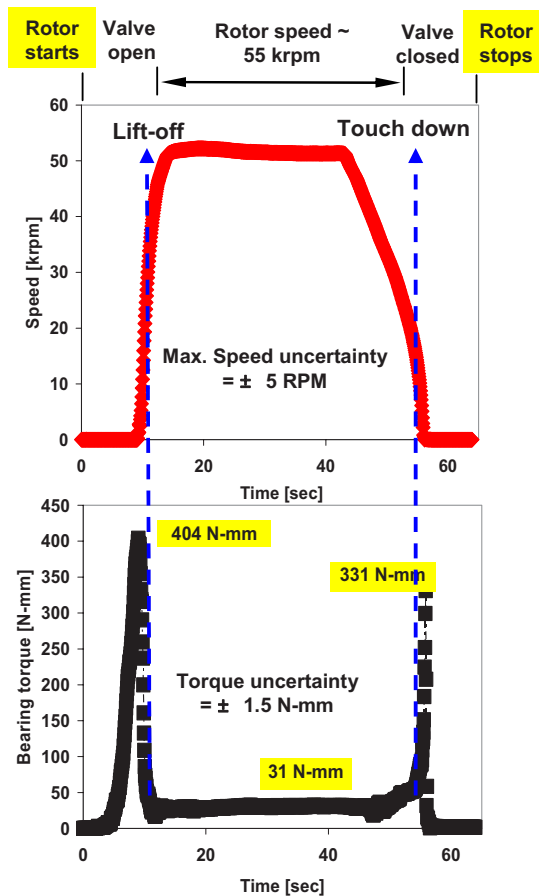


Fig. 10 Test data for journal speed and foil bearing drag torque versus time during a lift off and touch down cycle. Applied external pull load = 53 N

Figure 11 depicts the measured drag torque (T_{or}) versus rotor speed (Ω) for the various loads (W) applied during start-up speed operation. Prior to rotor lift-off (see Fig. 12), the drag torque is high denoting a dry-friction sliding condition. Above the lift-off speed, the drag torque is quite small demonstrating a nearly friction-free operation. Note that the maximum applied load (53 N) is about five times the bearing assembly weight (10.27 N).

Figure 12 shows that the identified rotor lift off and touch down speeds increase linearly with the applied load. San Andrés et al. [20] find similar results with a metal mesh foil bearing. Presently, note that the rotor touch down speed is about 4 krpm higher than the rotor lift off speed. This is not

unexpected due to thermal effects which quickly reduce the operating clearance so that the journal seizes into its bearing.

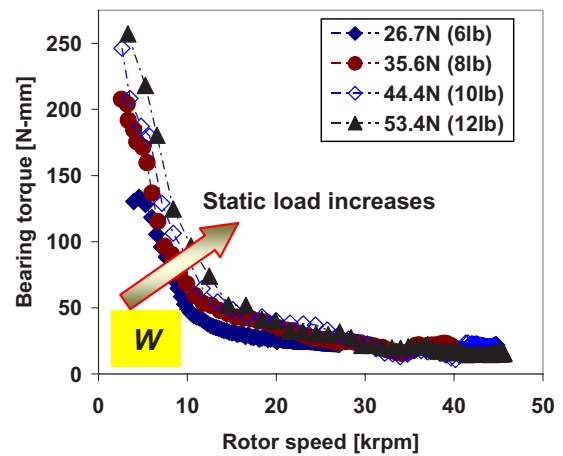


Fig. 11 GFB test data: Drag torque versus rotor speed for increasing static loads. Torque uncertainty = ± 3.9 N-mm.

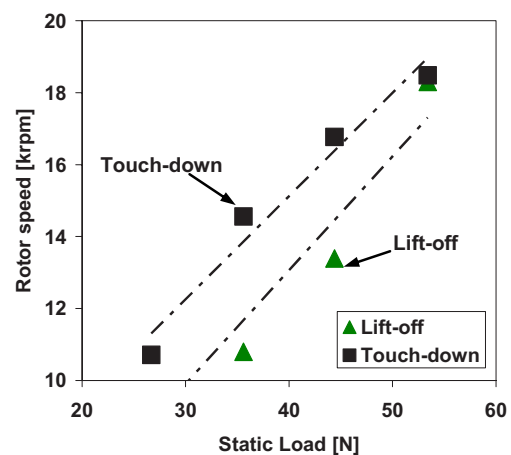


Fig. 12 GFB test data: Rotor lift off and touch down speeds versus static load. Uncertainty in load = ± 0.2 N

Figure 13 shows that the recorded peak drag torque, corresponding to a dry-friction sliding condition, is also proportional to rotor speed. In general, the break away drag torque just before the rotor lifts off is higher than the (stall) drag torque during a touch down condition. Note that the repeatability of the torque measurements is within 16% of the magnitude hereby reported.

A rotational drag friction coefficient, $f = T_{or} / (WR)$, is derived from the test data in Fig. 11 and $R = \frac{1}{2}D = 18.272$ mm as the journal radius. In Fig. 14, the friction coefficient, decreasing quickly with rotor speed, is particularly low once airborne operation is established. Note also that f decreases as the static load increases, denoting a more favorable operating regime. Figure 15 shows the calculated power loss for the test GFB, $\dot{\phi} = T_{or} \Omega$, versus rotor speed. Once the

rotor is airborne, operation above (say) 15 krpm, the drag power loss is rather low, < 100 W, for most loads applied.

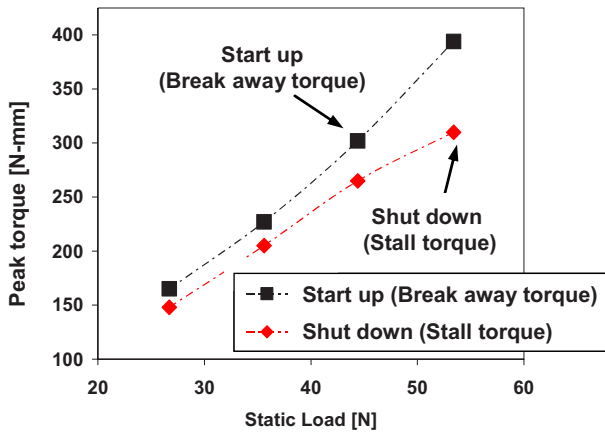


Fig. 13 GFB test data: Peak drag torque versus static load during start up (breakaway) and shut down (stall) events. Torque corresponds with dry-friction sliding

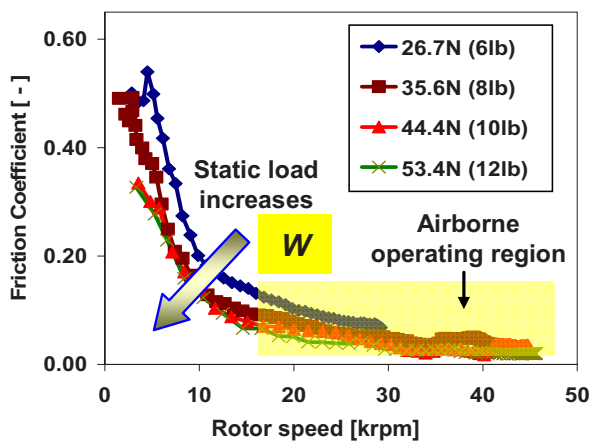


Fig. 14 GFB test data: Rotational drag friction coefficient (f) versus rotor speed for increasing static loads. Uncertainty in friction coefficient = ± 0.018

Recorded bearing cartridge temperatures at an outboard location are monitored to assess the bearing health condition. Figure 16 shows the bearing ID temperature versus rotor speed for increasing static loads. The temperature is measured at the free end of the bearing with a thermocouple glued on the ID of the bearing shell. The temperature reported represents continuous operation at the specified load and rotor speed. Temperature measurements show no distinctive trends, except that operation with the highest load $W=53$ N causes a large temperature raise, in particular at the lowest operating speed, ~ 24 krpm, just above the rotor lift-off speed.

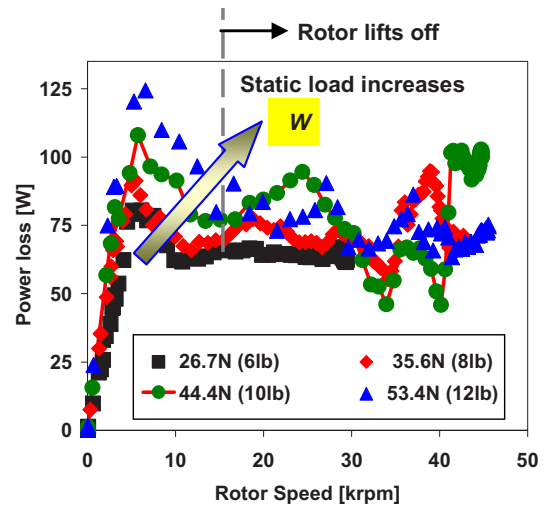


Fig. 15 Estimated drag power loss for first generation test GFB versus rotor speed and increasing static loads. Uncertainty in power loss = ± 12 W

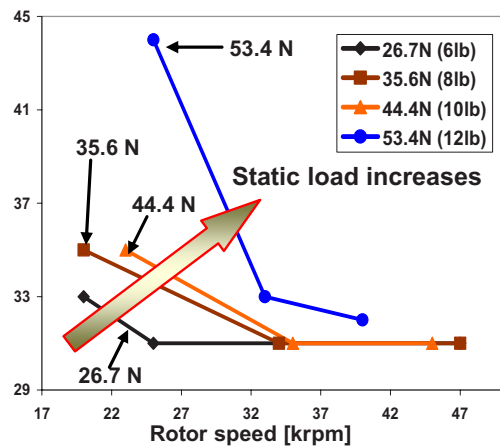


Fig. 16 GFB airborne test data: Bearing ID temperature versus rotor speed and increasing static loads. Ambient temperature at 21 °C

Figure 17 depicts photographs evidencing the surface condition of the journal and foil bearing after about 200+ start-stop cycles. For comparison, the figure includes the original pristine condition of both mechanical components. Note that the soft PTFE coating, 16 μ m thick, applied to the journal outer surface is entirely removed. There is even solid material wear since the journal (average) outer diameter reduced to 36.506 mm, from its original (uncoated) OD of 36.512 mm. The top foil also evidences polishing marks, in particular at its free end side. These polishing marks, most evident at the location where the bumps contact the top foil, are typical in foil bearings since there is insignificant hydrodynamic pressure generation in this zone. In spite of the severe journal wear, with a subsequent change in the FB operating clearance, the condition of the FB is deemed adequate for further operation.

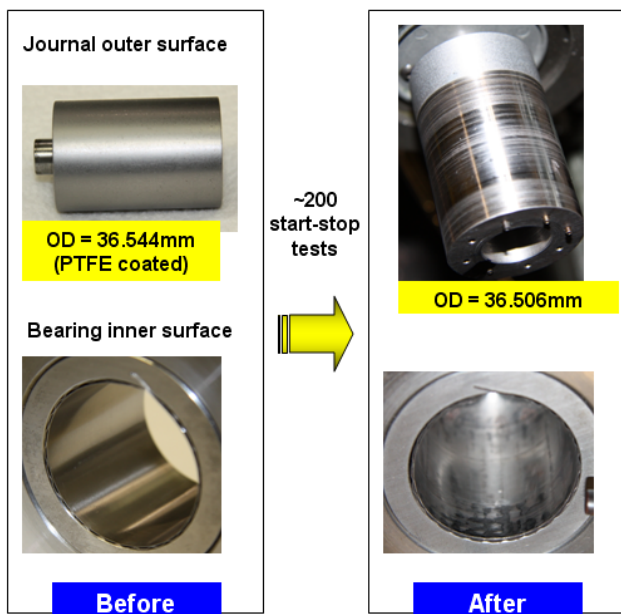


Fig. 17 Original and post-test condition of journal and test foil bearing

CONCLUSIONS

Analytical tools predicting foil bearing performance are yet to adequately address important issues such as lift off speed and drag torque as well as ultimate load capacity. Hence, empirical characterization of foil bearings prior to their field application is mandatory. The paper presents experiments conducted with a first generation foil bearing (FB) to identify its structural parameters (stiffness and damping) and to measure the bearing drag torque and lift off and shut down journal speeds while in operation under increasing applied static loads. The test procedure hereby described is both fast and cost efficient.

From the dynamic load tests with controlled FB displacement amplitudes, the bearing structural stiffness, ranging from 0.3 to 0.6 MN/m, increases with excitation frequency above the test system natural frequency. The mechanical energy dissipation in a FB is modeled as either of viscous type or structural type. The viscous damping coefficient drops quickly with excitation frequency, as is typical in mechanical systems with dry-friction. The loss factor, representing material or structural damping, decreases with frequency, and its magnitude at 0.3 and lesser denotes the limited damping characteristics of the first generation test foil bearing.

Experiments conducted with the FB mounted on a rotating journal driven by a turbocharger turbine show that the foil bearing drag torque peaks just before the journal lifts during a start-up event. The journal lift off speed and break away torque are proportional to the applied load on the FB. The bearing stall torque during a shut down event is typically ~20% lesser than during the start up condition. Once the rotor lifts, the bearing torque is minimal, remaining fairly constant regardless of the load applied, even for increasing journal speeds. The FB drag friction coefficient derived from the measured torque and applied load is largest for the smallest load condition. While operating at a constant speed

of 30krpm the friction coefficient is ~0.1 for all loads applied. Hence, power losses to drive the bearing remain relatively constant at just 100 W or less. The identified friction coefficient is somewhat larger than that obtained for a metal mesh foil bearing in Ref. [8].

Monitoring of the bearing cartridge temperature evidences a notable temperature raise, most significant for the highest load acting on the test bearing. Post-test inspection of the journal and test FB after 200+ cycles of start up and shut down events reveals that the layer of soft PTFE coating applied on the journal has disappeared, while the bearing has its top foil polished with signs of wear marks on its outboard side.

The education of the students in the emerging field of distributed power generation addresses to the current and future needs of a technology and knowledge driven society. The research gave an opportunity to engineering undergraduate students to experience and to contribute to a state of the art technology development program. Upon graduation, the novice engineers will hopefully pursue advanced studies in emerging applications of energy conservation and power generation.

ACKNOWLEDGEMENTS

This study is supported by National Science Foundation under REU#0552885 Program. The leadership of Dr. Wayne Hung, TAMU Engineering Technology Professor and Principal Investigator of NSF REUP, is hereby recognized. Projects from NASA GRC (agreement NNX07P98A) and the Turbomachinery Research Consortium (TRC) support the graduate students' research. Thanks to KIST for donating the test foil bearing.

Shane Muller, assisted by Keun Ryu, worked on dynamic load tests applied to one foil bearing to identify its structural stiffness and mechanical energy dissipation characteristics. José Camero, assisted by Thomas Chirathadam and Keun Ryu, operated a TC driven air turbine rig to measure FB drag torque (break away and stall) and rotor lift off speed during fast rotor startup and shut down events.

The first author wrote the paper based on edited posters prepared by the REUP students.

REFERENCES

1. DellaCorte, C., Radil, K. C., Bruckner, R. J. and Howard, S. A., Design, Fabrication, and Performance of Open Source Generation I and II Compliant Hydrodynamic Gas Foil Bearings, *STLE Tribol. Trans.*, Vol.51, No.3 (2008), pp. 254-264.
2. Lubell, D., DellaCorte, C. and Stanford, M., Test Evolution and Oil-Free Engine Experience of a High Temperature Foil Air Bearing Coating, *Proc. ASME Turbo Expo 2006*, Paper No. GT2006-90572, Barcelona, Spain, May (2006).
3. Chen, H. M., Howarth, R. Geren, B., Theilacker, J. C. and Soyars, W. M., Application of Foil Bearings to Helium Turbocompressor, *Proc. 30th Turbomachinery Symposium*, Turbomachinery Laboratory, Texas A&M University, Houston, TX, (2000), pp. 103-113.
4. Rubio, D. and San Andrés, L., Bump-Type Foil Bearing Structural Stiffness: Experiments and Predictions, *ASME J. Eng. Gas Turbines Power*, Vol.128 (2006), pp. 653-660.
5. Rubio, D. and San Andrés, L., Structural Stiffness, Dry Friction Coefficient, and Equivalent Viscous Damping in a Bump-Type Foil Gas Bearing, *ASME J. Eng. Gas Turbines Power*, Vol.129

- (2007), pp. 494-502.
6. Kim, T. H., Breedlove, A. W. and San Andrés, L., Characterization of a Foil Bearing Structure at Increasing Temperatures: Static Load and Dynamic Force Performance, *ASME J. Tribol.*, Vol.131(2009), p. 041703.
 7. San Andrés, L. and Ryu, K., Experimental Structural Stiffness and Damping In a 2nd Generation Foil Bearing for Increasing Shaft Temperatures, *Proc. 2009 ASME/STLE Int. Joint Tribology Conference*, Extended Abstract No. IJTC 2009-15188, Memphis, TN, Oct. (2009).
 8. San Andrés, L., Chirathadam, T. A. and Kim, T.H., Measurements of Structural Stiffness and Damping Coefficients in a Metal Mesh Foil Bearing, *ASME J. Eng. Gas Turbines Power*, Vol.132 (2010), p. 032503.
 9. San Andrés, L., Rubio, D. and Kim, T.H, Rotordynamic Performance of a Rotor Supported on Bump Type Foil Gas Bearings: Experiments and Predictions, *ASME J. Eng. Gas Turbines Power*, Vol.129 (2007), pp. 850–857.
 10. San Andrés, L. and Kim, T.H., Forced Nonlinear Response of Gas Foil Bearing Supported Rotors, *Trib. Int.*, Vol.41 (2008), pp. 704-715.
 11. Kim, T. H. and San Andrés, L., Effect of Side End Pressurization on the Dynamic Performance of Gas Foil Bearings – A Model Anchored to Test Data, *ASME J. Eng. Gas Turbines Power*, Vol.131 (2009), p. 012501.
 12. Kim, T.H. and San Andrés, L., Effects of a Mechanical Preload on the Dynamic Force Response of Gas Foil Bearings - Measurements and Model Predictions, *STLE Tribol. Trans.*, Vol.131 (2009), pp. 569-580.
 13. San Andrés, L. and Kim, T.H., Thermohydrodynamic Model Predictions and Performance Measurements of Bump-type Foil Bearing for Oil-Free Turbohaft Engines in Rotorcraft Propulsion Systems, *ASME J. Tribology*, Vol.132 (2010), p. 011701.
 14. San Andrés, L. and Kim, T. H., Thermohydrodynamic Analysis of Bump Type Gas Foil Bearings: A Model Anchored to Test Data, *ASME J. Eng. Gas Turbines Power*, Vol.132 (2010), p. 042504.
 15. San Andrés, L., Kim, T.H., Ryu, K., Chirathadam, T. A., Hagen, K., Martinez, A., Rice, B., Niedbalski, N., Hung, W. and Johnson, M., Gas Bearing Technology for Oil-Free Microturbomachinery – Research Experience for Undergraduate (REU) Program at Texas A&M University, *Proc. ASME Turbo Expo 2009*, Paper No. GT2009-59920, Orlando, Florida, Jun. (2009).
 16. San Andrés, L., Kim, T.H. and Ryu, K., “Thermohydrodynamic Analysis of Bump Type Gas Foil Bearings: A Model Anchored to Test Data,” *Quarter Progress Report #6 (Appendix A)*, to *NASA SSRW2-1.3 Oil Free Engine Technology Program*, Feb. (2009), Texas A&M University, College Station, TX
 17. San Andrés, L., Modern Lubrication Theory, Lecture Notes 14: Experimental Identification of Bearing Force Coefficients, 39 p., Open Source: <http://rotorlab.tamu.edu/TRIBGROUP> (July 23, 2009).
 18. San Andrés, L., Kim, T.H. and Ryu, K., “Thermohydrodynamic Analysis of Bump Type Gas Foil Bearings: A Model Anchored to Test Data,” *Quarter Progress Report #7 (Appendix M)*, to *NASA SSRW2-1.3 Oil Free Engine Technology Program*, May (2009), Texas A&M University, College Station, TX.
 19. Ginsberg, J., *Mechanical and Structural Vibrations*, (2001), Wiley, NY. pp. 137–139,
 20. San Andrés, L., Kim, T.H., Chirathadam, T.A. and Ryu, K., Measurements of Drag Torque, Lift-Off Journal Speed and Temperature in a Metal Mesh Foil Bearing, *American Helicopter Society 65th Annual Forum*, Grapevine, Texas, May (2009).
 21. Wilde, D., San Andrés, L. and Aguirrezabala, J., Experimental Lift Off Characteristics and the Effect of a Low Friction Coating on the Startup Response of Simple Gas Hybrid Bearings for Oil-Free Turbomachinery, *Proc. ASME Turbo Expo 2004*, Paper No. GT2004-54183, Vienna, Austria, Jun. (2004).